Cell Reports

Article

Pain-induced adaptations in the claustro-cingulate pathway

Graphical abstract

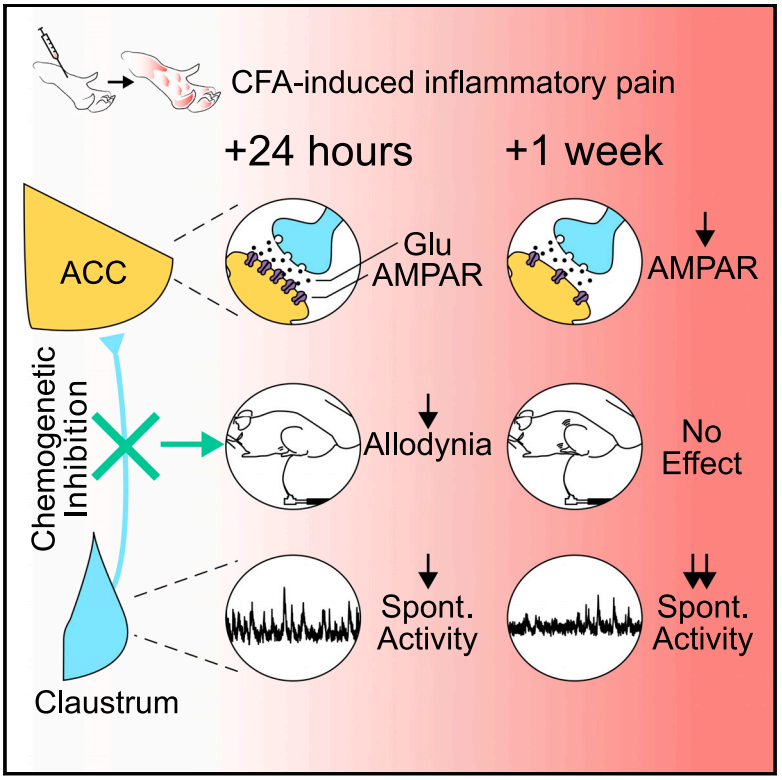

Highlights

- Inhibition of ACC-projecting claustrum (CLA_{ACC}) neurons reduces acute inflammatory allodynia
- CLA_{ACC} neurons preferentially represent aversive over more neutral stimuli
- Persistent pain impairs the modulation of ACC activity and inflammatory allodynia by the CLA
- Pain-induced claustrum-ACC decoupling involves a decrease in synaptic AMPA receptors

Authors

Niels R. Ntamati, Mario A. Acuña, Thomas Nevian

Correspondence

thomas.nevian@unibe.ch

In brief

The anterior cingulate cortex (ACC) receives nociceptive inputs from multiple brain regions. Ntamati et al. describe a population of claustrum neurons projecting to the ACC displaying preferential responses to aversive stimuli. Furthermore, they reveal the pain-modulatory role of this pathway along with its progressive functional impairment during persistent inflammatory pain.

Ntamati et al., 2023, Cell Reports *42*, 112506
May 30, 2023
https://doi.org/10.1016/j.celrep.2023.112506

CellPress

Cell Reports

CellPress
OPEN ACCESS

Article

Pain-induced adaptations in the claustro-cingulate pathway

Niels R. Ntamati,[1] Mario A. Acuña,[1] and Thomas Nevian[1,2,*]
[1]Department of Physiology, University of Bern, Bühlplatz 5, 3012 Bern, Switzerland
[2]Lead contact
*Correspondence: thomas.nevian@unibe.ch
https://doi.org/10.1016/j.celrep.2023.112506

SUMMARY

Persistent pain is a prevalent medical concern correlating with a hyperexcitable anterior cingulate cortex (ACC). Its activity is modulated by inputs from several brain regions, but the maladjustments that these afferent circuits undergo during the transition from acute to chronic pain still require clarification. We focus on ACC-projecting claustrum (CLA_{ACC}) neurons and their responses to sensory and aversive stimuli in a mouse model of inflammatory pain. Using chemogenetics, *in vivo* calcium imaging, and *ex vivo* electrophysiological approaches, we reveal that suppression of CLA_{ACC} activity acutely attenuates allodynia and that the claustrum preferentially transmits aversive information to the ACC. With prolonged pain, a claustro-cingulate functional impairment develops, which is mediated by a weakened excitatory drive onto ACC pyramidal neurons, resulting in a diminished claustral influence on the ACC. These findings support an instrumental role of the claustrum in the processing of nociceptive information and its susceptibility to persistent pain states.

INTRODUCTION

Throughout one's life, potentially harmful stimuli are continuously detected by peripheral nociceptors and contextually evaluated in the central nervous system to safely regulate behavior or, when said regulation fails, to generate the subjective sensory and emotional experience we call "pain."[1] Normally, pain manifests acutely and subsides with the resolution of the initial noxious insult. Its persistence, however, leads 1 in 5 people globally to the development of chronic pain syndromes that can last for years, are often poorly managed, and drastically reduce the patient's quality of life.[2]

Decades of research have established the involvement of prefrontal regions such as the anterior cingulate cortex (ACC) in the representation, encoding, and processing of the affective-motivational aspects of pain.[3–6] Rodent studies of ACC function have deepened our understanding of the cellular adaptations characterizing the chronic pain state and highlighted the emergence of aberrant plasticity mechanisms altering the strength of ACC afferents.[7–9] Recent tracing studies identified widespread inputs to the ACC originating from the claustrum, a thin, elongated nucleus sheathed between the striatum and the insular cortex.[10–12] Establishing reciprocal connections with all frontal cortical areas and, to a lesser extent, most sensorimotor cortices, the claustrum was proposed to support the salience network in detecting attention-worthy stimuli,[10] but its association with the ACC in relation to the processing of aversive and nociceptive stimuli and the development of chronic pain states is unknown.

The increased claustral activation in patients experiencing cognitively and emotionally exaggerated pain sensations (i.e., pain catastrophizing), as well as the report of paresthesias when it is electrically stimulated, suggests its possible contribution to the processing of pain and its aversive quality.[13,14] Additionally, enhanced pain thresholds in claustrum-lesioned animals and higher cFos expression with capsaicin-induced hypersensitivity further support this structure's involvement in pain encoding and expression.[15,16] This inferential evidence prompted our hypothesis that claustrum subpopulations associated with pain-relevant cortical areas might contribute to the processing and expression of the pain experience.

In the present article, we employ a retrograde viral approach to examine ACC-projecting claustral neurons and investigate their ability to represent aversive stimuli and to modulate nociceptive responses in a mouse model of inflammatory pain. Using *in vivo* 2-photon calcium imaging and *ex vivo* patch-clamp recordings, we expose a functional and synaptic weakening of the claustro-cingulate pathway, which emerges a week after prolonged pain. In sum, our results add to the growing body of evidence implicating the claustrum in sensory perception and behavioral regulation. We additionally speculate that the observed pain-induced alterations could contribute to the maladaptive changes within the attentional neural circuitry occurring during persistent pain states.

RESULTS

Claustro-cingulate pathway silencing acutely modulates allodynia

To assess whether the claustro-cingulate pathway can modulate pain responses, we first injected a retrograde adeno-associated viral vector expressing Cre-mCherry and expressed a Cre-dependent $G_{i/o}$-coupled hM4D receptor fused with mCitrine in

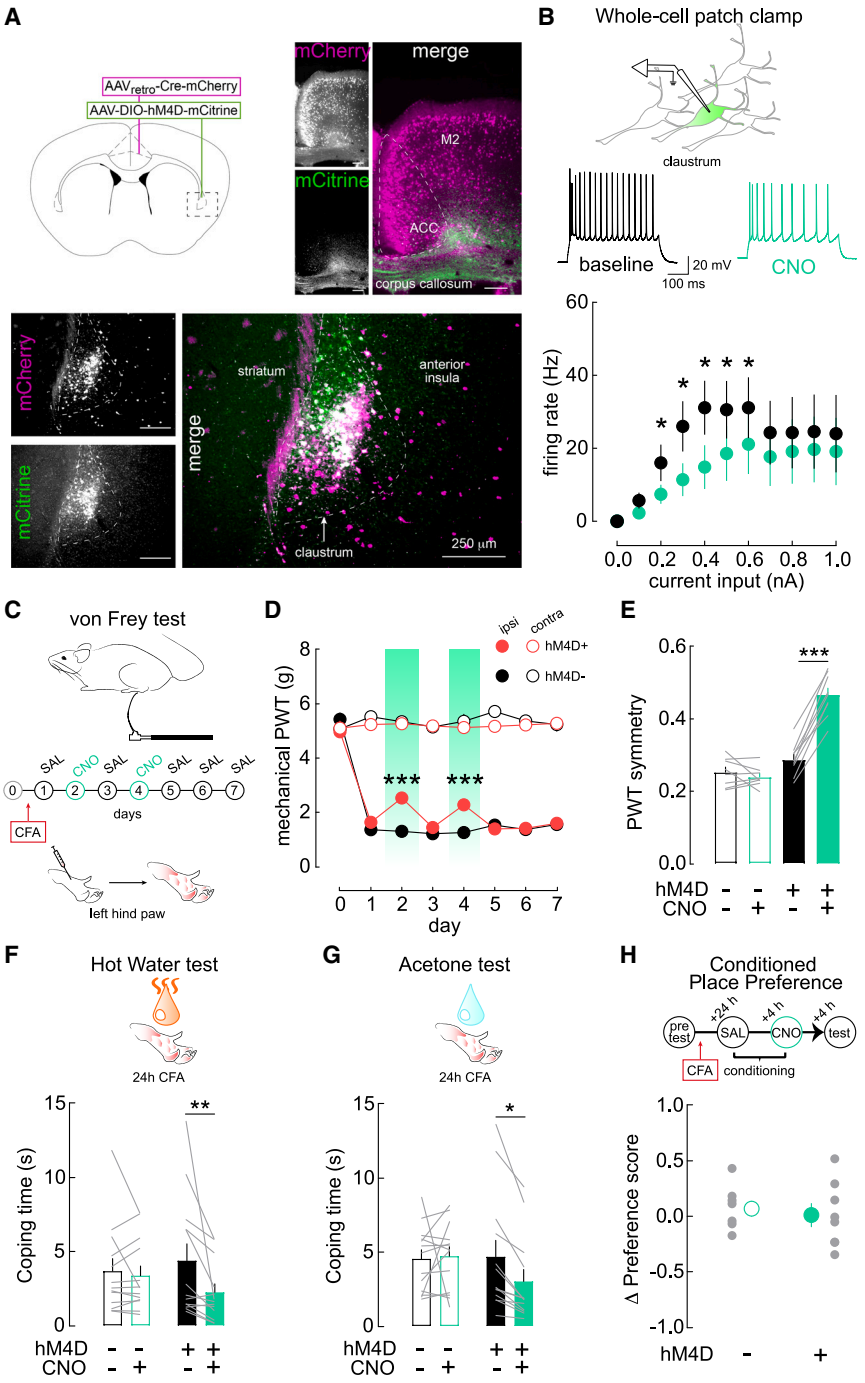

Figure 1. Suppression of CLA_{ACC} neuronal activity reduces allodynia

(A) Top left: viral targeting strategy to express hM4D-mCitrine in CLA_{ACC} neurons. Top right: injection site of Cre-mCherry (magenta)- and hM4D-mCitrine-expressing axons (green) in the ACC. Bottom: retrograde expression of Cre-mCherry- and Cre-dependent expression of hM4D-mCitrine in the claustrum.

(B) Top: whole-cell current clamp recordings of hM4D-mCitrine-expressing CLA_{ACC} neurons and example trace showing action potential firing in response to a 0.5 nA square current injection at baseline and after 10 μM CNO bath application. Bottom: input-output curve showing mean action potential firing rate as a function of injected current in CLA_{ACC} neurons before and after 10 μm CNO bath application (n = 7 neurons; two-way ANOVA: current injection × hM4d stimulation interaction, $p < 0.05$; Fisher's least significant difference [LSD], *$p < 0.05$).

(C) Schematic of von Frey protocol for quantification of CFA-induced mechanical allodynia following saline or CNO injections (2 mg/kg, i.p.).

(D) Time course of mechanical paw withdrawal thresholds (PWTs) following intraplantar CFA injection (30 μL) for both ipsilateral and contralateral paws in hM4D-positive mice and hM4D-negative controls (N = 8, 9 mice; two-way ANOVA: time point × hM4D expression interaction, $p < 0.001$; Bonferroni test: hM4D positive vs. hM4D negative, ***$p < 0.001$).

(E) Average PWT symmetry (ratio of ipsi- and contralateral PTWs) for saline- and CNO-administration days in hM4D-positive mice and hM4D-negative controls (N = 8, 9 mice; three-way-ANOVA: hM4D expression × time × hindpaw inflammation interaction, $p < 0.01$; Fisher's LSD: hM4D positive vs. hM4D negative, ***$p < 0.001$).

(F) Average duration of coping responses to the application of hot water on the acutely inflamed hindpaw of hM4D-positive mice and hM4D-negative controls. Mice were tested following i.p. saline or CNO administration (N = 13, 13 mice; two-way ANOVA: CNO treatment effect, *$p < 0.05$; Fisher's LSD: hM4D-positive saline vs. CNO, **$p < 0.01$).

(G) Average duration of coping responses to the plantar application of acetone, as in (F) (N = 13, 13 mice; two-way ANOVA: CNO treatment × hM4D expression interaction, *$p < 0.05$; Fisher's LSD: hM4D-positive saline vs. CNO, *$p < 0.05$).

(H) Top: timeline of the place conditioning protocol. Bottom: average change in preference score for the CNO-conditioned chamber in hM4D-positive mice and hM4D-negative controls. Gray points indicate values for individual mice (N = 8, 8 mice; Mann-Whitney U test, $p > 0.05$). Data are presented as mean ± SEM.

the claustrum (Figure 1A). This strategy allowed us to pharmacologically manipulate ACC-projecting claustrum (CLA_{ACC}) neurons with the hM4D ligand clozapine-N-oxide (CNO). *Ex vivo* whole-cell recordings from mCitrine-expressing CLA_{ACC} neurons confirmed their decreased excitability following bath application of 10 μM CNO (Figure 1B). We chose the complete Freund's adjuvant (CFA) inflammatory pain model to reliably provoke mechanical allodynia and thermal hyperalgesia in the left hind paw of hM4D-expressing mice and mCherry-expressing controls. Their mechanical paw sensitivity was measured daily with an electronic von Frey aesthesiometer following alternated intraperitoneal (i.p.) injections of either saline solution or 2 mg/kg CNO for the first 4 days post-CFA inoculation. Testing proceeded for 3 additional days with further saline injections to

observe potential carry-over effects from the last CNO dose (Figure 1C). Following the CFA-induced hypersensitization of the inflamed paw (ipsi), assessed by a decreased paw withdrawal threshold (PWT), we found that the hM4D group, but not mCherry controls, exhibited an elevated PWT on days when CNO was administered (Figure 1D). Importantly, this effect was not seen on the non-inflamed paw (contra) and led to a robust improvement of the PWT symmetry score (ratio of ipsi and contra PWTs), implying that it was not a consequence of a non-specific CNO-induced motor impairment (Figure 1E).

To examine the potential modulation of nocifensive responses to heat and cold (e.g., paw flinching, biting, and licking) after 1 day of CFA-induced pain, we measured the duration of these coping behaviors following the application of 0.1 mL of either hot water (80°C–85°C) or acetone on the inflamed hindpaw of hM4D-expressing mice and mCherry controls. We tested the animals after administering saline and CNO in two separate sessions and found that only hM4D-expressing mice reduced their coping times in the presence of CNO during thermal testing with hot water and acetone (Figures 1F and 1G). We finally investigated whether CNO could attenuate spontaneous as well as evoked pain responses. To this end, hM4D- and mCherry-expressing mice were allowed to freely explore a classical conditioned place preference apparatus (pretest) before receiving an intraplantar CFA injection. Twenty-four hours later, animals were conditioned in each chamber with either saline or CNO and later were allowed to freely explore the apparatus again. We quantified the relative change in time spent in the CNO-conditioned chamber during the test compared with the pretest (Δ preference score), where positive values would indicate an increased preference for the CNO-paired chamber (over the saline-paired one), hinting at a rewarding effect of the CLA_{ACC} circuit inhibition. Contrary to these assumptions, CNO did not increase the preference score for the paired chamber, producing similar effects in both hM4D mice and mCherry controls (Figure 1H), suggesting that this circuit manipulation did not influence the CFA-induced ongoing pain. Additionally, we did not detect any locomotor differences among mice undergoing saline or CNO conditioning, further ruling out a motor impairment as an explanation for the CNO effects (Figure S1). From these results, we concluded that CLA_{ACC} neuronal suppression can acutely and reversibly modulate mechanical and thermal nociception while leaving spontaneous ongoing pain unaffected, implicating this pathway in the behavioral expression of stimulus-evoked inflammatory allodynia.

CLA_{ACC} neuronal responses to aversive sensory stimulation

Because of its effect on the inflamed, but not the healthy, paw (Figure 1D), we reasoned that the chemogenetic inhibition of CLA_{ACC} neurons could have interfered with the processing of pain-relevant information. Activity within claustrum neurons is modulated by a variety of sensory stimuli.[17,18] It is unknown, however, whether aversive stimuli are represented within claustral networks interacting with pain-responsive cortical areas. To this end, we retrogradely labeled CLA_{ACC} neurons with Cre-mCherry and transduced them with the Cre-dependent fluorescent calcium indicator GCaMP6f. This allowed us to visualize the activity-related calcium dynamics of CLA_{ACC} neurons through an implanted gradient index (GRIN) lens *in vivo* with a 2-photon microscope (Figure 2A). We performed our recordings under light anesthesia (0.5%–1% isoflurane), which precluded us from measuring correlates of the conscious pain experience but nonetheless allowed for the examination of the inherent stimulus-specific activity of the claustrum, unaffected by cognitive and premotor preprocessing. In these conditions, we were able to reliably record the spontaneous activity of CLA_{ACC} neurons (Figure 2B) as well as the calcium responses to three sensory stimuli with distinct aversive qualities. An electric foot shock (FS), an air puff (AP) directed to the eye, and a white-noise (WN) sound burst were used, respectively, as strongly, mildly, and weakly aversive stimuli, all leading to varying degrees of evoked calcium activity (Figure 2C). We found that, among 385 recorded CLA_{ACC} neurons, most cells exhibited significant responses to a single stimulus rather than to multiple ones (34.3% and 12.5%, respectively), with FS-responsive neurons accounting for the largest proportion of selectively activated cells (Figure 2D). This subpopulation had faster peak responses and was activated for a longer duration than AP- or WN-responsive neurons (Figures 2 E, 2F, S2A, and S2B). Additionally, FS-responsive neurons exhibited significantly larger stimulus-evoked calcium responses, despite overall similar levels of spontaneous activity (Figures 2 G, 2H, S2C, and S2D). Altogether, these results confirm the existence of sensory-related neuronal responses in the claustrum and suggest that the claustro-cingulate pathway preferentially reacts to noxious information over less aversive stimuli.

Inflammatory pain-driven changes in the claustrum

Given their aversive representation capacity and pain behavior modulation, we wondered whether a prolonged pain state would alter the representation of noxious information within CLA_{ACC} neurons over time. We followed the single-cell calcium activity of CLA_{ACC} neurons in naive, healthy conditions (day 0), as well as 24 h (day 1) and 1 week (day 7) after an intraplantar injection of saline or CFA, to examine the temporal stability of their stimulus representations (Figure 3A). In both inflamed animals and saline controls, we detected considerable dynamic fluctuations in the single-cell stimulus selectivity across recording days (Figure 3B), reminiscent of the temporal variance in stimulus representation already described in other cortical areas.[19,20] Analyzing this representational drift between saline- and CFA-injected mice, we tested whether inflammatory pain could influence the relative selectivity to a specific stimulus but found that the overall proportions of FS, AP, and WN responses oscillated similarly between saline- and CFA-injected mice (Figures S3A–S3C). We then classified the recorded neurons according to their stable, changed, lost, or gained stimulus-responding properties, again finding proportionally similar changes in the first 24 h (Figure 3C). Conversely, we observed that twice as many CLA_{ACC} neurons lost their stimulus selectivity after 1 week of inflammatory pain compared with saline controls (Figure 3D). Nonetheless, the average FS-elicited responses remained stable across days and were similar between healthy and inflamed animals (Figures 3A and 3E). Similarly, all

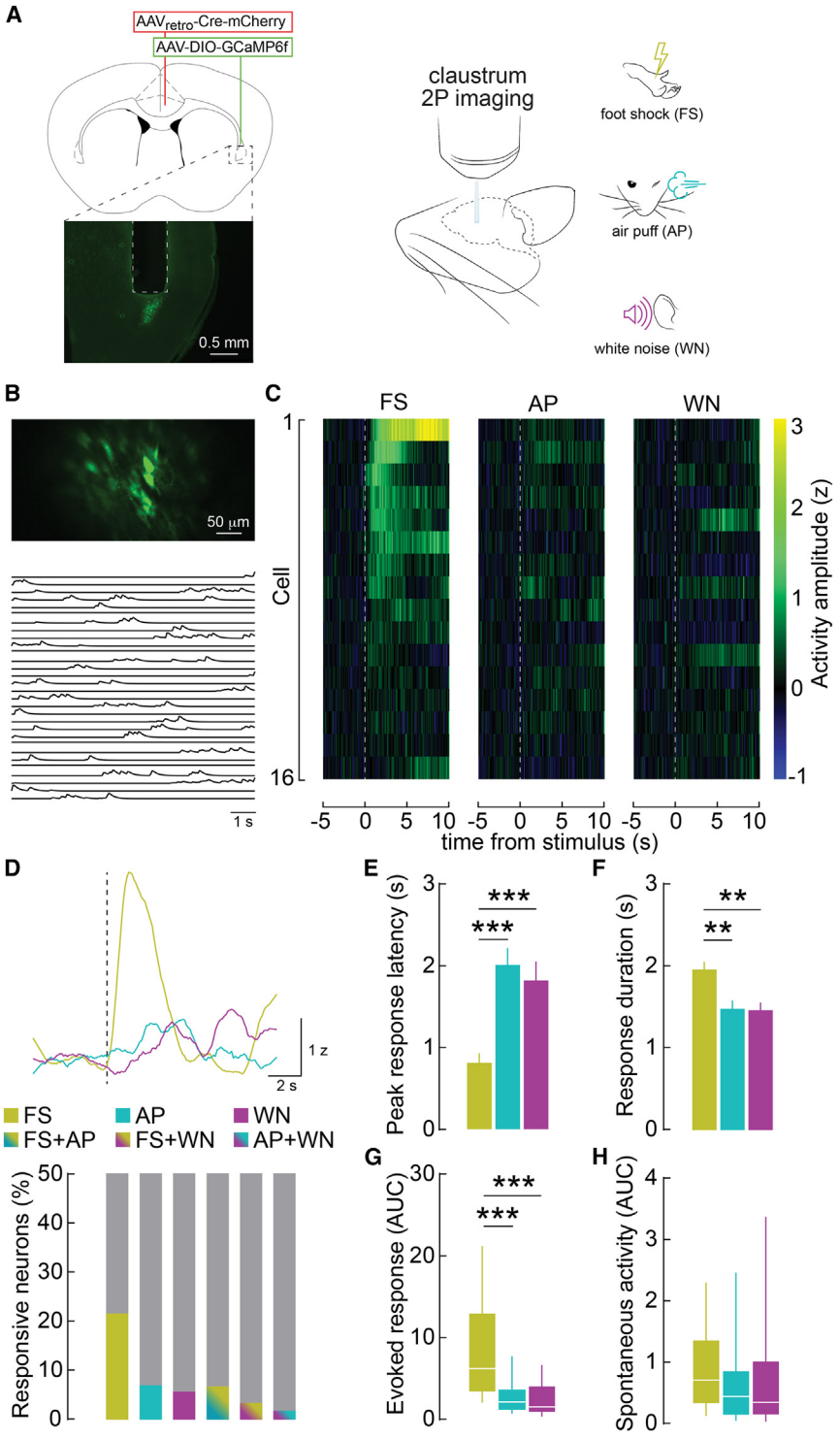

Figure 2. *In vivo* CLA_{ACC} responses to aversive sensory stimuli

(A) Viral targeting strategy for the Cre-dependent expression of GCaMP6f in CLA_{ACC} neurons and histological verification of GRIN lens implantation above the claustrum. GCaMP6f-expressing neurons are imaged under a 2-photon microscope to record their spontaneous activity as well as foot shock (FS)-, air puff (AP)-, and white noise (WN)-related activity.

(B) Field of view and spontaneous calcium activity in a sample CLA_{ACC} neuron.

(C) *Z*-scored peristimulus activity heatmap of stimulus-evoked responses from the neurons shown in (B). Neurons are ordered by mean FS-evoked activity.

(D) Top: example *Z* scored calcium traces from a neuron responding to FS but not AP or WN. Bottom: proportion of recorded neurons exhibiting significant calcium responses to one or more stimuli.

(E) Average latency to peak calcium responses, highlighting faster activations for FS-responsive neurons compared with AP- and WN-responsive neurons (n = 128, 66, 48 neurons, N = 12 mice; one-way ANOVA, $p < 0.001$; Bonferroni test, ***$p < 0.001$) (see Figure S2A for individual data points).

(F) Longer duration of calcium activity above baseline levels in FS-responsive neurons compared with AP- and WN-responsive neurons (n = 128, 66, 48 neurons, N = 12 mice; one-way ANOVA, $p < 0.001$; Bonferroni test, **$p < 0.01$) (see Figure S2B for individual data points).

(G) Area under the curve of stimulus-evoked calcium responses showing larger activations in FS-responsive neurons (n = 128, 66, 48 neurons, N = 12 mice; one-way ANOVA, $p < 0.001$; Bonferroni test, ***$p < 0.001$) (see Figure S2C for individual data points).

(H) Similar area under the curve of spontaneous calcium activity for all stimuli-responsive neurons (n = 128, 66, 48 neurons, N = 12 mice; one-way ANOVA, $p > 0.05$) (see Figure S2D for individual data points). Data are presented as mean ± SEM or median with interquartile range and outliers.

stimulus-evoked calcium responses were unaffected by inflammatory pain (Figures S3D–S3F), although we surprisingly noticed a gradual decline in the average spontaneous activity of CLA_{ACC} neurons following CFA injection, whereas saline controls maintained stable activity levels (Figures 3F and S3G). Whole-cell recordings from CLA_{ACC} neurons *ex vivo* showed that 1 week of inflammatory pain did not alter their rheobase, input resistance, or input-output relationship (Figures S3H–S3K), suggesting that their lowered spontaneous activity *in vivo* might arise from modifications in network activity rather than intrinsic excitability. Taken together, these findings show how sensory stimuli can be dynamically processed at the single-cell level in the claustrum while being stably represented at the population level. Additionally, the decreased spontaneous activity and larger loss of stimulus selectivity indicate that persistent pain may be associated with a gradual degradation of the information-encoding properties of claustral networks.

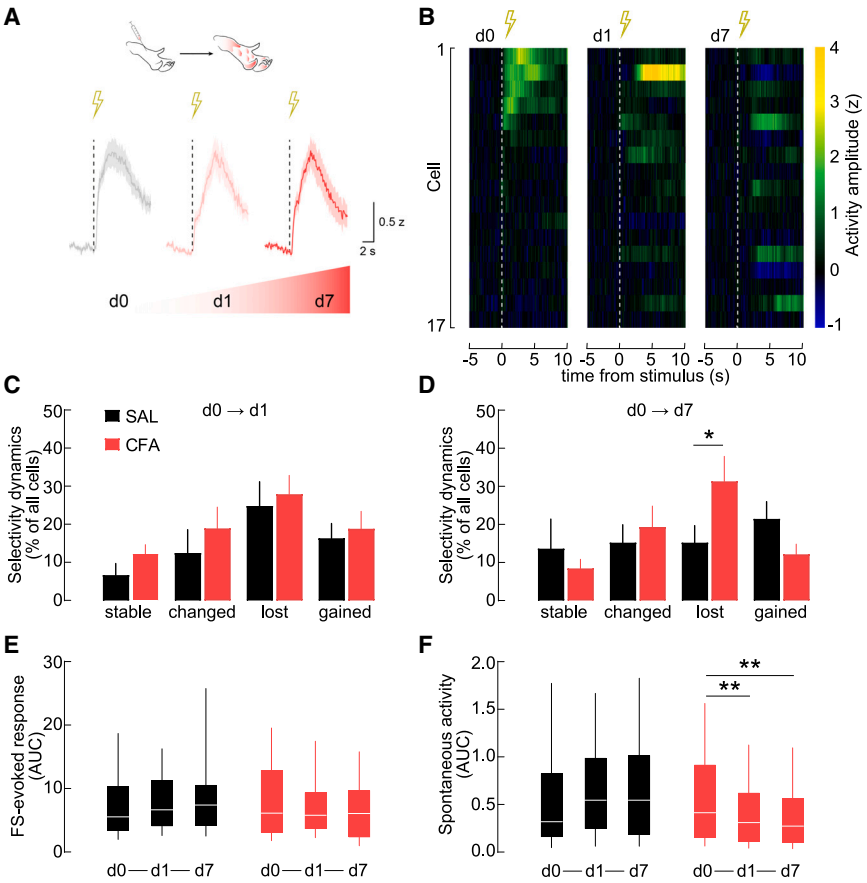

Figure 3. CLA_{ACC} neuronal responses during inflammatory pain

(A) Illustration of average FS-elicited calcium responses in naive conditions and during inflammatory pain.

(B) *Z*-scored peristimulus activity heatmap of FS-evoked responses from a sample field of view across three time points. Neurons are ordered by mean FS-evoked activity on day 0.

(C) Percentage of recorded neurons exhibiting distinct selectivity dynamics from days 0 to 1, showing similar changes between saline- and CFA-injected mice. (N = 4, 6 mice; two-way ANOVA, $p > 0.05$).

(D) Percentage of recorded neurons exhibiting distinct selectivity dynamics from days 0 to 7, highlighting a larger proportion of lost stimulus-selectivity in CFA-injected mice (two-way ANOVA, $p > 0.05$; Fisher's LSD, $^{*}p < 0.05$).

(E) Area under the curve of FS-evoked responses across time shows stable evoked responses following saline or CFA injection (n = 35, 39 neurons, N = 4, 6 mice; repeated measures two-way ANOVA, $p > 0.05$) (see Figure S3D for individual data points).

(F) Spontaneous activity decrease in CLA_{ACC} neurons across time following CFA, but not saline, injection (n = 74, 82 neurons, N = 4, 6 mice; repeated measures two-way ANOVA: pain state × time interaction, $p < 0.01$; Bonferroni's test, $^{**}p < 0.01$) (see Figure S3G for individual data points). Data are presented as mean ± SEM or median with interquartile range and outliers.

Prolonged pain reduces ACC excitatory drive from the claustrum

Previous studies have suggested that claustral activation generally leads to the inhibition of its cortical targets' principal cells through the activation of local interneurons.[21–23] Yet, since ACC activity positively correlates with the perceived unpleasantness of pain,[24,25] we reasoned that the outcome of our claustrocingulate manipulation rather reflected the excitatory nature of this pathway (Figures 1E and 1F). To test this hypothesis and gauge the net influence of claustrum projections on the ACC, we expressed the hM4D receptor in CLA_{ACC} neurons and transduced ACC pyramidal neurons with a CaMKIIα promoter-driven GCaMP6f. In lightly anesthetized mice, implanted with a GRIN lens above the ACC, we imaged pyramidal neurons at baseline and following i.p. injections of either saline or 2 mg/kg CNO and calculated the single-cell change in calcium activity (Figure 4A). In naive mice, the CNO-mediated suppression of CLA_{ACC} inputs led to a significantly larger decrease in both spontaneous and stimulus-evoked activity of ACC pyramidal neurons compared with saline-injected controls. This reduction was preserved in the first 24 h of CFA-induced inflammatory pain but not at later stages (1 week of CFA), when we found that CLA_{ACC} inhibition was no longer able to significantly modulate ACC activity (Figures 4B–4E and S4A–S4D). These results establish the existence of a tonic excitatory influence of the claustrum on the ACC, which is lost at 1 week of inflammatory pain. We therefore investigated whether such functional deficit would manifest behaviorally by examining the PWT symmetry in an additional cohort of mice expressing hM4D in CLA_{ACC} neurons (as in Figure 1). We performed repeated von Frey testing after i.p. injections of saline (sessions 1 and 3) or CNO (session 2) to evaluate the effect of silencing the CLA_{ACC} pathway after 1 week of inflammatory pain (Figure 4F). Consistent with the observed loss of ACC modulation, CNO lost its ability to improve the PWT symmetry or the coping responses to thermal stimuli in hM4D-expressing mice after 1 week of persistent pain (Figures 4G–4H, S4E, and S4F), supporting a relation between the claustrum's influence on the ACC and its modulation of nocifensive responses.

Claustrum-ACC synaptic alterations after 1 week of inflammatory pain

The deteriorated ACC sensitivity to claustral modulation could originate from direct glutamatergic CLA_{ACC} inputs progressively losing strength during prolonged pain states. Alternatively, claustral neurons might exert their effects through a heterogeneous projection pattern onto ACC pyramidal neurons and networks of local interneurons. The CFA-induced loss of claustrum-ACC coupling could thus be achieved by shifting the relative weight of these excitatory (direct) and inhibitory (indirect) inputs. To explore these possibilities, we injected mice with a

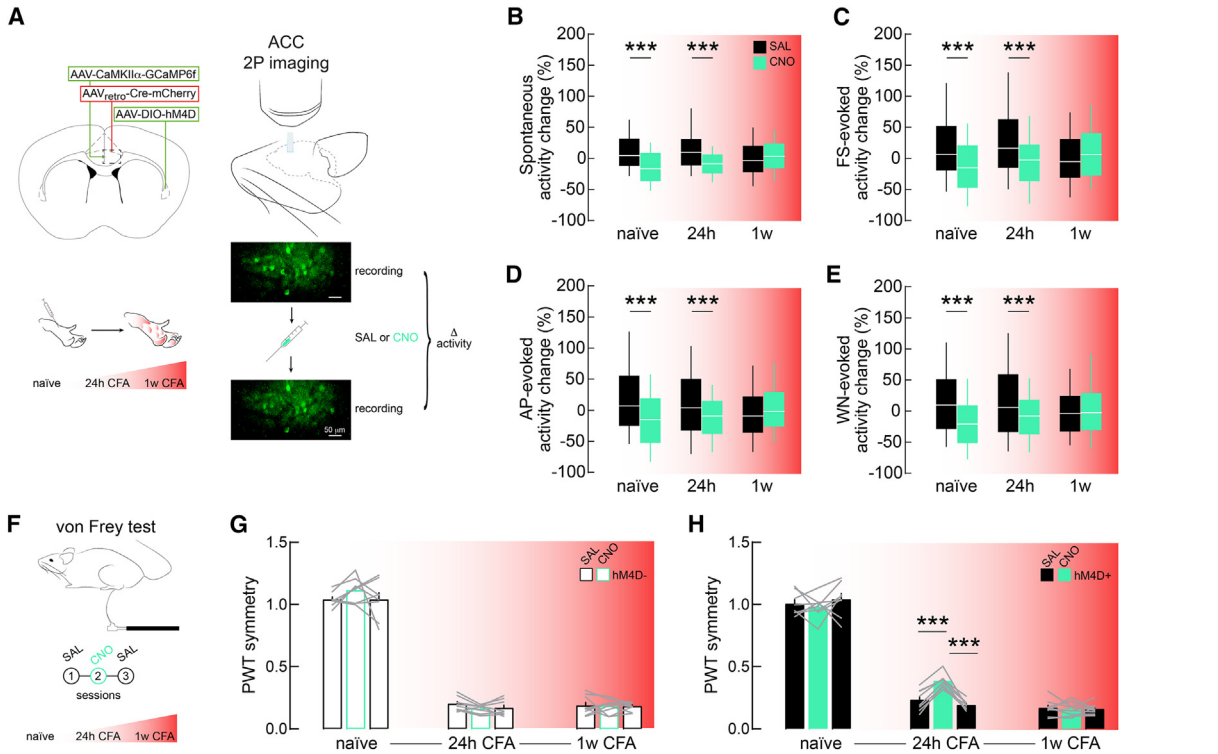

Figure 4. Loss of ACC modulation by the claustrum after prolonged pain

(A) Viral targeting strategy to Cre-dependently express hM4D-mCitrine in CLA_{ACC} neurons and GCaMP6f in ACC pyramidal neurons. Neuronal responses are recorded under a 2-photon microscope before and after a saline or CNO injection to quantify the activity change in the ACC following CLA_{ACC} inhibition.

(B) Percentage change in spontaneous activity after saline or CNO treatment at different time points of CFA-induced inflammatory pain. In both naive and 24 h CFA conditions (but not 1 week CFA), ACC neuronal activity was lower in the presence of CNO (n = 242–341 neurons, N = 8, 8 mice; two-way ANOVA: time in pain × CNO treatment interaction, $p < 0.001$; Fisher's LSD, ***$p < 0.001$) (see Figure S4A for individual data points).

(C–E) Percentage change in FS-, AP-, and WN-evoked activity between saline- and CNO-treated mice. As in (B), ACC neuronal activity was suppressed by CNO compared with saline in naive and 24 h CFA conditions but not at 1 week CFA (n = 242–341 neurons, N = 8, 8 mice; two-way ANOVA: time in pain × CNO treatment interaction, $p < 0.001$; Fisher's LSD, ***$p < 0.001$) (see Figures S4B–S4D for individual data points).

(F) Protocol for repeated von Frey testing after alternated saline and CNO injections in naive mice and following inflammatory pain induction. Mice underwent three testing sessions (following i.p. saline, CNO, and saline again) at all pain conditions (naive, 24 h CFA, and 1 week CFA).

(G and H) PWT symmetry in hM4D-negative and hM4D-positive mice measured in naive conditions and during early and late inflammatory pain following saline or CNO administration. While hM4D-negative mice were unaffected by CNO treatment (G), hM4D-positive neurons increased their PWT symmetry at 24 h CFA (H) but not at 1 week CFA or naive conditions (N = 8, 8 mice; repeated measures one-way ANOVA hM4D-positive: 24 h CFA, $p < 0.01$; Bonferroni's test, *$p < 0.05$). Data are presented as mean ± SEM or median with interquartile range and outliers.

retrograde Cre-mCherry-encoding virus in the ACC to conditionally express the light-gated ion channel ChR2 in the claustrum and to optically probe CLA_{ACC} inputs onto ACC layer 5 pyramidal neurons with *ex vivo* whole-cell patch-clamp recordings (Figure 5A). ChR2-expressing axonal terminals were stimulated with blue light pulses to elicit fast excitatory postsynaptic currents (EPSCs) that were abolished by the sodium channel blocker tetrodotoxin (TTX) and subsequently rescued by the potassium channel blocker 4-aminopyridine (4-AP; Figure S2A), confirming the monosynaptic nature of this connection.[26] Stimulation of CLA_{ACC} terminals also evoked inhibitory postsynaptic currents (IPSCs) sensitive to the $GABA_A$ receptor antagonist gabazine (Figures 5B and S2B). These IPSCs displayed longer onset latencies and, like EPSCs, were eliminated by antagonizing glutamate receptors with CNQX and AP5 (Figures 5C and S2C), confirming the direct glutamatergic innervation of ACC pyramidal neurons by CLA_{ACC} projections, together with a slower and indirect inhibitory input mediated by local interneurons. We thus calculated the ratio of EPSCs to IPSCs as a measure of excitation/inhibition balance, finding it unaltered between mice that had received an intraplantar injection of either saline or CFA 1 week earlier (Figure 5D). In contrast, the paired-pulse ratio (PPR) of IPSCs was significantly increased in CFA animals, indicating a moderate short-term facilitatory shift in these strongly depressing inhibitory synapses (Figure 5E). EPSCs, on the other hand, did not display CFA-induced changes in short-term plasticity (Figure 5F). We observed, however, that the relative contribution of AMPA to NMDA currents was reduced after a week of inflammatory pain compared with saline controls (Figures 5G and 5H). Although a decreased AMPA-to-NMDA ratio could be explained by an increased synaptic insertion of inwardly rectifying GluA2-lacking AMPA receptors, we observed similar degrees of inward rectification between saline and CFA animals, rejecting this hypothesis (Figure 5I). Similarly, NMDA receptor

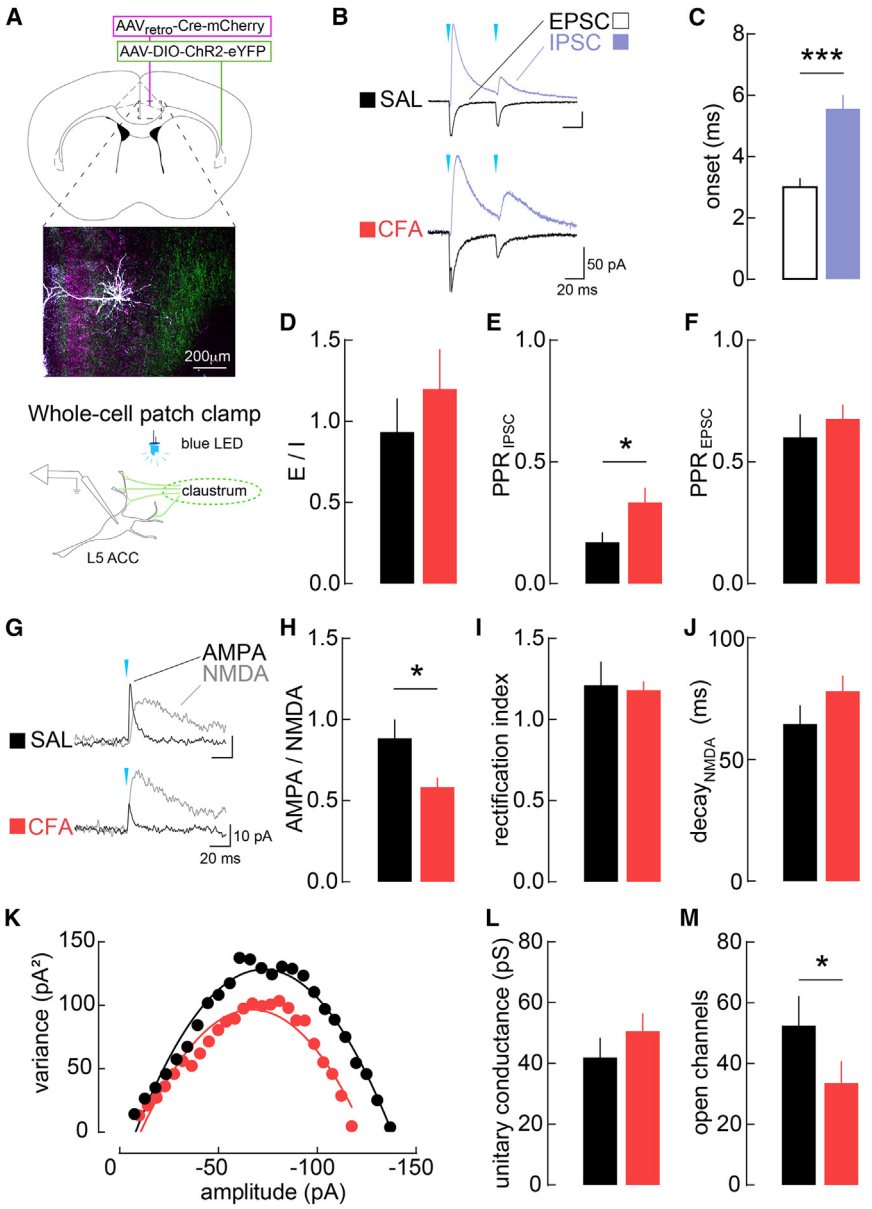

Figure 5. Synaptic weakening of claustrum inputs to L5 ACC pyramidal neurons after 1 week of inflammatory pain

(A) Viral targeting of CLA_{ACC} neurons to express ChR2-EYFP and sample biocytin-filled neuron recorded in layer 5 ACC 1 week after intraplantar CFA injection.

(B) Example traces recorded in ACC-containing brain slices 1 week after saline or CFA treatment. EPSCs and IPSCs were recorded at holding potentials of −70 and 0 mV, respectively. Arrowheads indicate blue light stimulation of ChR2-expressing axons.

(C) Mean onset latency for EPSCs and IPSCs, showing fast excitatory, and slower inhibitory, responses onto L5 ACC pyramidal neurons (n = 21 neurons; Wilcoxon signed-rank test, $p < 0.001$).

(D) Ratios of EPSCs over IPSCs show similar excitation/inhibition balance in saline- and CFA-injected animals (n = 17, 21 neurons; N = 8, 8 mice; Mann-Whitney U test, $p > 0.05$).

(E–F) Paired-pulse ratios for IPSCs (n = 16, 19 neurons; Mann-Whitney U test, $p < 0.05$) and EPSCs (n = 17, 22 neurons; N = 8, 8 mice; Mann-Whitney U test, $p > 0.05$), showing a change in short-term plasticity on inhibitory, but not excitatory, synapses after 1 week of CFA-induced pain.

(G) Example traces recorded at +40 mV to isolate AMPA and NMDA receptor-mediated currents in saline- and CFA-treated mice.

(H) AMPA-to-NMDA receptor-mediated current ratio after 1 week of saline or CFA-induced pain (n = 19, 20 neurons; N = 9, 8 mice; Mann-Whitney U test, $p < 0.05$).

(I) Mean AMPA receptor rectification index (ratio of negative and positive AMPA chord conductances) (n = 13, 14 neurons; N = 9, 8 mice; Mann-Whitney U test, $p > 0.05$).

(J) Mean decay kinetics of NMDA receptors remain stable after 1 week of CFA-induced pain (n = 17, 15 neurons; N = 9, 8 mice; Mann-Whitney U test, $p > 0.05$).

(K) Mean amplitude-variance relationship obtained from the non-stationary fluctuation analysis of AMPA EPSCs. A parabolic fit of the current variance data is used to obtain estimates of unitary channel conductance and number of open channels (see STAR Methods).

(L) Mean unitary conductance of AMPA receptors remains stable between saline- and CFA-injected mice (n = 17, 19 neurons; N = 8, 7 mice; Mann-Whitney U test, $p > 0.05$).

(M) Mean number of open AMPA receptors is decreased 1 week following CFA administration (Mann-Whitney U test, $p < 0.05$). Data are presented as mean ± SEM.

decay kinetics remained comparable between groups, also ruling out alterations that could have arisen from NMDA subunit changes (Figure 5J). We lastly performed a non-stationary fluctuation analysis[27] to estimate the synaptic number and single-channel conductance of AMPA receptors from the parabolic relationship between their mean current amplitude and the associated current variance around the mean (Figure 5K). Consistent with the stable rectification index, we found the single-channel conductance unchanged following 1 week of inflammatory pain, whereas the number of open AMPA channels was significantly lowered compared with saline controls (Figures 5L and 5M). Collectively, the present results describe a reduction in AMPA-mediated glutamatergic efficacy onto L5 ACC pyramidal neurons, together with a relative facilitation of local inhibition, as possible synaptic mechanisms contributing to the impaired claustrum-ACC coupling emerging during prolonged pain states.

DISCUSSION

The claustrum, as well as the ACC, has been implicated in sensory processing and in the modulation of attentional processes.[18,28–31] The present work consolidates the sensory representational properties of the claustrum and provides direct

evidence for the preferential processing of strongly aversive information over more neutral stimuli within a subpopulation of ACC-projecting (CLA_{ACC}) neurons.

Despite the low concentrations used in this study, the volatile anesthetic isoflurane is known to suppress "top-down" cortico-cortical network activity, while "bottom-up" thalamocortical information transfer is less affected.[32] We could therefore reliably observe calcium responses to distinct sensory stimulations under light anesthesia, with electrical FS responses being more robustly represented than APs or WN sound bursts. This preparation presumably allowed us to investigate the passive stimulus responses in the claustrum without potential confounds coming from learned premotor activity that might arise from repeated stimulation in an awake, conscious animal.[17,33] It remains to be tested, however, whether the response amplitudes, proportions of responding neurons, and selectivity dynamics would be comparable in freely moving mice.

Suppression of CLA_{ACC} activity during early stages of inflammatory pain was able to acutely alleviate the hypersensitized responses to somatic stimulation, suggesting a role for this circuit in the behavioral expression of mechanical allodynia and thermal hyperalgesia. Importantly, the same manipulation was not able to produce negative reinforcement from pain relief in CFA-injected animals, suggesting that different circuits are involved in the modulation of spontaneous and evoked pain.[34] This could arise from an altered cortical processing of external noxious stimuli leading to, or modulating, the expression of nocifensive reflexes and coping behaviors. In humans, the ACC is consistently activated by noxious stimulation, and its functional connectivity with descending pain modulatory areas correlates with prolonged pain intensity.[35,36] Similarly, in rodents, the ACC is crucial for pain aversion learning and the expression of nociceptive behavioral responses.[24,37] Consistent with these studies, our results establish an excitatory functional role for CLA_{ACC} projections in driving the ACC to support allodynia. While this coupling involves both a direct excitation of layer 5 pyramidal neurons and their feedforward inhibition through local GABAergic interneurons, our imaging data demonstrate an overall decrease in excitatory tone in the ACC following CLA_{ACC} inhibition. Interestingly, *in vivo* extracellular recordings performed by Jackson and colleagues indicated an inhibitory, rather than excitatory, functional coupling between the claustrum and the medial prefrontal cortex (mPFC), which lies just adjacent to the ACC.[22] This difference likely arises from area- and layer-specific claustral projection patterns onto networks of pyramidal neurons and local inhibitory interneurons, whose interplay may steer toward either cortical excitation or inhibition. Because of the extensive collateralization of frontal-projecting claustral neurons,[10,38] it is reasonable to expect that our manipulation of CLA_{ACC} neurons concurrently led to the disinhibition of some mPFC principal neurons. Unlike in the ACC, pyramidal activity in the prelimbic mPFC correlates positively with antinociception and is reduced during chronic pain states.[39–41] Therefore, our modulation of mechanical allodynia might derive from the concerted response of distinct brain areas, beyond the ACC, being differentially regulated by the claustrum and converging to a common behavior. It remains to be tested whether the claustral influence over prelimbic neurons also undergoes similar pain-related adaptations as observed in the ACC.

Previous research on the information-encoding properties of the claustrum revealed its ability to represent internal premotor activity as well as external sensory events. These studies, however, could not examine the temporal stability of these neuronal representations. Indeed, several associational and sensory cortical areas do not always show stable stimulus-related neuronal responses but can display a continuous reconfiguration of such representations, so that the encoding of information can vary within single neurons while often remaining stable at the population level.[19,42–44] Our findings similarly expose this representational drift in the claustrum, suggesting that information about sensory stimuli may be flexibly distributed across a dynamic subset of CLA_{ACC} neurons. Nonetheless, the average responses to all stimuli remained unchanged throughout all recording sessions and even across 1 week of inflammatory pain. This shows that, despite its ability to affect behavioral responses to noxious stimuli when silenced, CLA_{ACC} neuronal activity may not reflect the intensity of sensitized responses observed during pain chronification. Interestingly, we also found a higher proportion of CLA_{ACC} neurons losing their stimulus responsiveness after 1 week of inflammatory pain. Together with the observed decline in overall CLA_{ACC} spontaneous activity, this could imply that persistent pain states may degrade these neurons' ability to convey relevant aversive information to the ACC over time.

In parallel to these changes, our work reveals the functional decoupling between claustrum and ACC after 1 week of inflammatory pain, whereby CLA_{ACC} suppression no longer affects ACC pyramidal activity or CFA-induced mechanical allodynia. This deficit may arise from the depotentiation of AMPA receptor-mediated excitatory transmission onto layer 5 pyramidal neurons, which constitute the main cortical output layer.[45,46] While we did not observe pain-induced changes in the excitation/inhibition balance of the CLA_{ACC} neurotransmission, the synaptic facilitation of GABAergic feedforward inhibition during pain could theoretically provide an additional interference to the excitatory drive from the claustrum by supporting higher frequencies of tonic presynaptic inhibitory activity.[47]

The recent surge in claustrum studies has advanced several hypotheses about its possible functions—from salience detection and attention modulation to the regulation of impulsivity and slow-wave sleep.[28,48–50] Our findings add to this body of work by corroborating previous suggestions about the claustrum's involvement in pain.[15,51,52] Curiously, several lines of research support a close relationship between attention and pain wherein chronic pain states not only impair attentional performance[9,53] but could also be exacerbated by the excessive attention to, and anticipation of, nociceptive sensations.[54,55] It should also be noted that ACC neurons are not only activated by painful sensations but are also involved in response conflict and error detection—suggesting a broader function in tuning attention toward the most attention-grabbing stimuli during cognitively and emotionally demanding situations.[56–58] Since the claustrum was also proposed to support behavioral performance under cognitively demanding tasks,[59–61] we speculate that the claustro-cingulate pathway may play a role in

coordinating the activity of attentional and salience networks to regulate behavioral responses to aversive stimuli. Although the present study focused on the adaptations produced during the first week of inflammatory pain, it remains to be tested how these changes progress over a longer time frame and whether they serve as a compensatory mechanism to relieve the cognitive load in the ACC or rather follow the alteration in the claustrum's ability to regulate attention to nociceptive signals during the chronification of pain. Exploring the attention-modulating function of claustrum projection neurons, Atlan and colleagues demonstrated their critical role in filtering out distracting elements to efficiently support goal-directed behavioral performance in the presence of task-unrelated stimuli.[28] It is conceivable that the synaptic weakening and functional decoupling between claustrum and ACC activity might reflect one's progressive inability to disrupt attention from noxious stimuli when pain becomes persistent. Future investigations should therefore probe the association of persistent pain states and attentional deficits to determine the causal relation between pain-induced claustro-cingulate adaptations and behavioral performance.

Limitations of the study

As a first limitation, it should be acknowledged that only male mice were used in our study, which may limit the generalizability of our results. There is an urgent need to better understand the complex mechanisms underlying pain chronification in both sexes.[62] Sex differences in the perception of acute pain, the response to analgesia, and the manifestation of chronic pain are indisputable in the clinical practice, presumably due to genetic, hormonal, and environmental factors.[63–65] Nevertheless, the precise mechanisms on the cellular and circuit levels are less understood. Whether the claustrum differentially affects pain processing between sexes has yet to be determined. This might indeed be the case, as the claustrum was proposed to be supporting cognitive flexibility by controlling attentional set shifting,[66] a function that is impaired in male, more than in female, mice in chronic neuropathic pain.[67] Thus, not only does sexual dimorphism need to be elucidated, but also the influence of the claustrum on other chronic pain models ought to be studied. Another important limitation comes from our use of an indirect and non-contingent chemogenetic approach to assess the net excitatory effect of claustral projections to the ACC, as different stimulation patterns may give rise to distinct and more complex neuronal responses.[68] Finally, our use of a single injection into the ACC for retrograde tagging together with the inefficient Cre-dependent recombination led to incomplete targeting of the whole CLA_{ACC} subpopulation. While this may have restrained the effect size of our manipulations, our study provides nonetheless an important proof of principle about synaptic and functional impairments in the claustro-cingulate pathway induced by prolonged pain states.

STAR★METHODS

Detailed methods are provided in the online version of this paper and include the following:

- KEY RESOURCES TABLE
- RESOURCE AVAILABILITY
  - Lead contact
  - Materials availability
  - Data and code availability
- EXPERIMENTAL MODEL AND SUBJECT DETAILS
- METHOD DETAILS
  - Virus injections
  - Pain induction and behavioral testing
  - GRIN lens implantation
  - Two-photon microscopy
  - Electrophysiology
  - Histology
- QUANTIFICATION AND STATISTICAL ANALYSIS

SUPPLEMENTAL INFORMATION

Supplemental information can be found online at https://doi.org/10.1016/j.celrep.2023.112506.

ACKNOWLEDGMENTS

We are grateful to Dr. Paolo De Luna and Natalie Nevian for technical and analytical assistance. This work was supported by the Swiss National Science Foundation (T.N., grants 159872 and 182571) and the European Research Council (T.N., grant 682905).

AUTHOR CONTRIBUTIONS

Conceptualization, N.R.N., M.A.A., and T.N.; methodology, N.R.N., M.A.A., and T.N.; formal analysis, N.R.N. and M.A.A.; investigation, N.R.N.; writing – original draft, N.R.N. and T.N.; writing – review & editing, N.R.N., M.A.A., and T.N.; visualization, N.R.N.; project administration, T.N.; funding acquisition, T.N.

DECLARATION OF INTERESTS

The authors declare no competing interests.

Received: October 24, 2022
Revised: March 31, 2023
Accepted: April 27, 2023

REFERENCES

1. Apkarian, A.V. (2019). Definitions of nociception, pain, and chronic pain with implications regarding science and society. Neurosci. Lett. *702*, 1–2. https://doi.org/10.1016/j.neulet.2018.11.039.
2. Treede, R.-D., Rief, W., Barke, A., Aziz, Q., Bennett, M.I., Benoliel, R., Cohen, M., Evers, S., Finnerup, N.B., First, M.B., et al. (2015). A classification of chronic pain for ICD-11. Pain *156*, 1003–1007. https://doi.org/10.1097/j.pain.0000000000000160.
3. Baliki, M.N., Chialvo, D.R., Geha, P.Y., Levy, R.M., Harden, R.N., Parrish, T.B., and Apkarian, A.V. (2006). Chronic pain and the emotional brain: specific brain activity associated with spontaneous fluctuations of intensity of chronic back pain. J. Neurosci. *26*, 12165–12173. https://doi.org/10.1523/JNEUROSCI.3576-06.2006.
4. Price, D.D. (2000). Psychological and neural mechanisms of the affective dimension of pain. Science *288*, 1769–1772. https://doi.org/10.1126/science.288.5472.1769.
5. Rainville, P., Duncan, G.H., Price, D.D., Carrier, B., and Bushnell, M.C. (1997). Pain affect encoded in human anterior cingulate but not somatosensory cortex. Science *277*, 968–971. https://doi.org/10.1126/science.277.5328.968.

6. Falkowska, M., Ntamati, N.R., Nevian, N.E., Nevian, T., and Acuña, M.A. (2023). Environmental enrichment promotes resilience to neuropathic pain-induced depression and correlates with decreased excitability of the anterior cingulate cortex. Front. Behav. Neurosci. *17*, 1139205. https://doi.org/10.3389/fnbeh.2023.1139205.

7. Hogrefe, N., Blom, S.M., Valentinova, K., Ntamati, N.R., Jonker, L.J.E., Nevian, N.E., and Nevian, T. (2022). Long-lasting, pathway-specific impairment of a novel form of spike-timing-dependent long-term depression by neuropathic pain in the anterior cingulate cortex. J. Neurosci. *42*, 2166–2179.

8. Koga, K., Descalzi, G., Chen, T., Ko, H.-G., Lu, J., Li, S., Son, J., Kim, T., Kwak, C., Huganir, R.L., et al. (2015). Coexistence of two forms of LTP in ACC provides a synaptic mechanism for the interactions between anxiety and chronic pain. Neuron *85*, 377–389. https://doi.org/10.1016/j.neuron.2014.12.021.

9. Zhao, M.-G., Ko, S.W., Wu, L.-J., Toyoda, H., Xu, H., Quan, J., Li, J., Jia, Y., Ren, M., Xu, Z.C., and Zhuo, M. (2006). Enhanced presynaptic neurotransmitter release in the anterior cingulate cortex of mice with chronic pain. J. Neurosci. *26*, 8923–8930. https://doi.org/10.1523/JNEUROSCI.2103-06.2006.

10. Chia, Z., Augustine, G.J., and Silberberg, G. (2020). Synaptic connectivity between the cortex and claustrum is organized into functional modules. Curr. Biol. *30*, 2777–2790.e4. https://doi.org/10.1016/j.cub.2020.05.031.

11. White, M.G., Cody, P.A., Bubser, M., Wang, H.-D., Deutch, A.Y., and Mathur, B.N. (2017). Cortical hierarchy governs rat claustrocortical circuit organization. J. Comp. Neurol. *525*, 1347–1362. https://doi.org/10.1002/cne.23970.

12. Mathur, B.N. (2014). The claustrum in review. Front. Syst. Neurosci. *8*, 48. https://doi.org/10.3389/fnsys.2014.00048.

13. Bickel, S., and Parvizi, J. (2019). Electrical stimulation of the human claustrum. Epilepsy Behav. *97*, 296–303. https://doi.org/10.1016/j.yebeh.2019.03.051.

14. Gracely, R.H., Geisser, M.E., Giesecke, T., Grant, M.A.B., Petzke, F., Williams, D.A., and Clauw, D.J. (2004). Pain catastrophizing and neural responses to pain among persons with fibromyalgia. Brain *127*, 835–843. https://doi.org/10.1093/brain/awh098.

15. Persinger, M.A., Peredery, O., Bureau, Y.R., and Cook, L.L. (1997). Emergent properties following brain injury: the claustrum as a major component of a pathway that influences nociceptive thresholds to foot shock in rats. Percept. Mot. Skills *85*, 387–398. https://doi.org/10.2466/pms.1997.85.2.387.

16. Tan, L.L., Pelzer, P., Heinl, C., Tang, W., Gangadharan, V., Flor, H., Sprengel, R., Kuner, T., and Kuner, R. (2017). A pathway from midcingulate cortex to posterior insula gates nociceptive hypersensitivity. Nat. Neurosci. *20*, 1591–1601. https://doi.org/10.1038/nn.4645.

17. Chevée, M., Finkel, E.A., Kim, S.-J., O'Connor, D.H., and Brown, S.P. (2022). Neural activity in the mouse claustrum in a cross-modal sensory selection task. Neuron *110*, 486–501.e7. https://doi.org/10.1016/j.neuron.2021.11.013.

18. Remedios, R., Logothetis, N.K., and Kayser, C. (2010). Unimodal responses prevail within the multisensory claustrum. J. Neurosci. *30*, 12902–12907. https://doi.org/10.1523/JNEUROSCI.2937-10.2010.

19. Driscoll, L.N., Pettit, N.L., Minderer, M., Chettih, S.N., and Harvey, C.D. (2017). Dynamic reorganization of neuronal activity patterns in parietal cortex. Cell *170*, 986–999.e16. https://doi.org/10.1016/j.cell.2017.07.021.

20. Rule, M.E., Loback, A.R., Raman, D.V., Driscoll, L.N., Harvey, C.D., and O'Leary, T. (2020). Stable task information from an unstable neural population. Elife *9*, e51121. https://doi.org/10.7554/eLife.51121.

21. Crescimanno, G., Salerno, M.T., Cortimiglia, R., Amato, G., and Infantellina, F. (1984). Functional relationship between claustrum and pyramidal tract neurons, in the cat. Neurosci. Lett. *44*, 125–129. https://doi.org/10.1016/0304-3940(84)90069-7.

22. Jackson, J., Karnani, M.M., Zemelman, B.V., Burdakov, D., and Lee, A.K. (2018). Inhibitory control of prefrontal cortex by the claustrum. Neuron *99*, 1029–1039.e4. https://doi.org/10.1016/j.neuron.2018.07.031.

23. Ptito, M., and Lassonde, M.C. (1981). Effects of claustral stimulation on the properties of visual cortex neurons in the cat. Exp. Neurol. *73*, 315–320. https://doi.org/10.1016/0014-4886(81)90066-2.

24. Johansen, J.P., Fields, H.L., and Manning, B.H. (2001). The affective component of pain in rodents: direct evidence for a contribution of the anterior cingulate cortex. Proc. Natl. Acad. Sci. USA *98*, 8077–8082. https://doi.org/10.1073/pnas.141218998.

25. Qu, C., King, T., Okun, A., Lai, J., Fields, H.L., and Porreca, F. (2011). Lesion of the rostral anterior cingulate cortex eliminates the aversiveness of spontaneous neuropathic pain following partial or complete axotomy. Pain *152*, 1641–1648. https://doi.org/10.1016/j.pain.2011.03.002.

26. Petreanu, L., Huber, D., Sobczyk, A., and Svoboda, K. (2007). Channelrhodopsin-2–assisted circuit mapping of long-range callosal projections. Nat. Neurosci. *10*, 663–668. https://doi.org/10.1038/nn1891.

27. Benke, T.A., Lüthi, A., Isaac, J.T., and Collingridge, G.L. (1998). Modulation of AMPA receptor unitary conductance by synaptic activity. Nature *393*, 793–797. https://doi.org/10.1038/31709.

28. Atlan, G., Terem, A., Peretz-Rivlin, N., Sehrawat, K., Gonzales, B.J., Pozner, G., Tasaka, G.I., Goll, Y., Refaeli, R., Zviran, O., et al. (2018). The claustrum supports resilience to distraction. Curr. Biol. *28*, 2752–2762.e7. https://doi.org/10.1016/j.cub.2018.06.068.

29. Laurienti, P.J., Wallace, M.T., Maldjian, J.A., Susi, C.M., Stein, B.E., and Burdette, J.H. (2003). Cross-modal sensory processing in the anterior cingulate and medial prefrontal cortices. Hum. Brain Mapp. *19*, 213–223. https://doi.org/10.1002/hbm.10112.

30. Wu, D., Deng, H., Xiao, X., Zuo, Y., Sun, J., and Wang, Z. (2017). Persistent neuronal activity in anterior cingulate cortex correlates with sustained attention in rats regardless of sensory modality. Sci. Rep. *7*, 43101. https://doi.org/10.1038/srep43101.

31. Goll, Y., Atlan, G., and Citri, A. (2015). Attention: the claustrum. Trends Neurosci. *38*, 486–495. https://doi.org/10.1016/j.tins.2015.05.006.

32. Raz, A., Grady, S.M., Krause, B.M., Uhlrich, D.J., Manning, K.A., and Banks, M.I. (2014). Preferential effect of isoflurane on top-down vs. bottom-up pathways in sensory cortex. Front. Syst. Neurosci. *8*, 191.

33. Reus-García, M.M., Sánchez-Campusano, R., Ledderose, J., Dogbevia, G.K., Treviño, M., Hasan, M.T., Gruart, A., and Delgado-García, J.M. (2021). The claustrum is involved in cognitive processes related to the classical conditioning of eyelid responses in behaving rabbits. Cerebr. Cortex *31*, 281–300. https://doi.org/10.1093/cercor/bhaa225.

34. Navratilova, E., Xie, J.Y., Okun, A., Qu, C., Eyde, N., Ci, S., Ossipov, M.H., King, T., Fields, H.L., and Porreca, F. (2012). Pain relief produces negative reinforcement through activation of mesolimbic reward–valuation circuitry. Proc. Natl. Acad. Sci. USA *109*, 20709–20713. https://doi.org/10.1073/pnas.1214605109.

35. Apkarian, A.V., Bushnell, M.C., Treede, R.-D., and Zubieta, J.-K. (2005). Human brain mechanisms of pain perception and regulation in health and disease. Eur. J. Pain *9*, 463–484. https://doi.org/10.1016/j.ejpain.2004.11.001.

36. Meeker, T.J., Schmid, A.-C., Keaser, M.L., Khan, S.A., Gullapalli, R.P., Dorsey, S.G., Greenspan, J.D., and Seminowicz, D.A. (2022). Tonic pain alters functional connectivity of the descending pain modulatory network involving amygdala, periaqueductal gray, parabrachial nucleus and anterior cingulate cortex. Neuroimage *256*, 119278. https://doi.org/10.1016/j.neuroimage.2022.119278.

37. Gu, L., Uhelski, M.L., Anand, S., Romero-Ortega, M., Kim, Y.t., Fuchs, P.N., and Mohanty, S.K. (2015). Pain inhibition by optogenetic activation of specific anterior cingulate cortical neurons. PLoS One *10*, e0117746. https://doi.org/10.1371/journal.pone.0117746.

38. Ham, G.X., and Augustine, G.J. (2022). Topologically organized networks in the claustrum reflect functional modularization. Front. Neuroanat. *16*, 901807.

39. Wang, G.-Q., Cen, C., Li, C., Cao, S., Wang, N., Zhou, Z., Liu, X.-M., Xu, Y., Tian, N.-X., Zhang, Y., et al. (2015). Deactivation of excitatory neurons in the prelimbic cortex via Cdk5 promotes pain sensation and anxiety. Nat. Commun. *6*, 7660. https://doi.org/10.1038/ncomms8660.

40. Zhang, Z., Gadotti, V.M., Chen, L., Souza, I.A., Stemkowski, P.L., and Zamponi, G.W. (2015). Role of prelimbic GABAergic circuits in sensory and emotional aspects of neuropathic pain. Cell Rep. *12*, 752–759. https://doi.org/10.1016/j.celrep.2015.07.001.

41. Dale, J., Zhou, H., Zhang, Q., Martinez, E., Hu, S., Liu, K., Urien, L., Chen, Z., and Wang, J. (2018). Scaling up cortical control inhibits pain. Cell Rep. *23*, 1301–1313. https://doi.org/10.1016/j.celrep.2018.03.139.

42. Clopath, C., Bonhoeffer, T., Hübener, M., and Rose, T. (2017). Variance and invariance of neuronal long-term representations. Philos. Trans. R. Soc. Lond. B Biol. Sci. *372*, 20160161. https://doi.org/10.1098/rstb.2016.0161.

43. Marks, T.D., and Goard, M.J. (2021). Stimulus-dependent representational drift in primary visual cortex. Nat. Commun. *12*, 5169. https://doi.org/10.1038/s41467-021-25436-3.

44. Schoonover, C.E., Ohashi, S.N., Axel, R., and Fink, A.J.P. (2021). Representational drift in primary olfactory cortex. Nature *594*, 541–546. https://doi.org/10.1038/s41586-021-03628-7.

45. Baker, A., Kalmbach, B., Morishima, M., Kim, J., Juavinett, A., Li, N., and Dembrow, N. (2018). Specialized subpopulations of deep-layer pyramidal neurons in the neocortex: bridging cellular properties to functional consequences. J. Neurosci. *38*, 5441–5455. https://doi.org/10.1523/JNEUROSCI.0150-18.2018.

46. Larsen, D., Wickersham, I., and Callaway, E. (2008). Retrograde tracing with recombinant rabies virus reveals correlations between projection targets and dendritic architecture in layer 5 of mouse barrel cortex. Front. Neural Circ. *2*.

47. Jackman, S.L., and Regehr, W.G. (2017). The mechanisms and functions of synaptic facilitation. Neuron *94*, 447–464. https://doi.org/10.1016/j.neuron.2017.02.047.

48. Liu, J., Wu, R., Johnson, B., Vu, J., Bass, C., and Li, J.-X. (2019). The claustrum-prefrontal cortex pathway regulates impulsive-like behavior. J. Neurosci. *39*, 10071–10080. https://doi.org/10.1523/JNEUROSCI.1005-19.2019.

49. Narikiyo, K., Mizuguchi, R., Ajima, A., Shiozaki, M., Hamanaka, H., Johansen, J.P., Mori, K., and Yoshihara, Y. (2020). The claustrum coordinates cortical slow-wave activity. Nat. Neurosci. *23*, 741–753. https://doi.org/10.1038/s41593-020-0625-7.

50. Smith, J.B., Watson, G.D.R., Liang, Z., Liu, Y., Zhang, N., and Alloway, K.D. (2019). A role for the claustrum in salience processing? Front. Neuroanat. *13*, 64.

51. Atilgan, H., Doody, M., Oliver, D.K., McGrath, T.M., Shelton, A.M., Echeverria-Altuna, I., Tracey, I., Vyazovskiy, V.V., Manohar, S.G., and Packer, A.M. (2022). Human lesions and animal studies link the claustrum to perception, salience, sleep and pain. Brain *145*, 1610–1623. https://doi.org/10.1093/brain/awac114.

52. Xu, Q.-Y., Zhang, H.-L., Du, H., Li, Y.-C., Ji, F.-H., Li, R., and Xu, G.-Y. (2022). Identification of a glutamatergic claustrum-anterior cingulate cortex circuit for visceral pain processing. J. Neurosci. *42*, 8154–8168. https://doi.org/10.1523/JNEUROSCI.0779-22.2022.

53. Moore, D.J., Meints, S.M., Lazaridou, A., Johnson, D., Franceschelli, O., Cornelius, M., Schreiber, K., and Edwards, R.R. (2019). The effect of induced and chronic pain on attention. J. Pain *20*, 1353–1361. https://doi.org/10.1016/j.jpain.2019.05.004.

54. Crombez, G., Viane, I., Eccleston, C., Devulder, J., and Goubert, L. (2013). Attention to pain and fear of pain in patients with chronic pain. J. Behav. Med. *36*, 371–378. https://doi.org/10.1007/s10865-012-9433-1.

55. McCracken, L.M. (1997). Attention" to pain in persons with chronic pain: a behavioral approach. Behav. Ther. *28*, 271–284. https://doi.org/10.1016/S0005-7894(97)80047-0.

56. Braver, T.S., Barch, D.M., Gray, J.R., Molfese, D.L., and Snyder, A. (2001). Anterior cingulate cortex and response conflict: effects of frequency, inhibition and errors. Cerebr. Cortex *11*, 825–836. https://doi.org/10.1093/cercor/11.9.825.

57. Davis, K.D., Taylor, K.S., Hutchison, W.D., Dostrovsky, J.O., McAndrews, M.P., Richter, E.O., and Lozano, A.M. (2005). Human anterior cingulate cortex neurons encode cognitive and emotional demands. J. Neurosci. *25*, 8402–8406. https://doi.org/10.1523/JNEUROSCI.2315-05.2005.

58. Newman, L.A., and McGaughy, J. (2011). Attentional effects of lesions to the anterior cingulate cortex: how prior reinforcement influences distractibility. Behav. Neurosci. *125*, 360–371. https://doi.org/10.1037/a0023250.

59. White, M.G., Mu, C., Qadir, H., Madden, M.B., Zeng, H., and Mathur, B.N. (2020). The mouse claustrum is required for optimal behavioral performance under high cognitive demand. Biol. Psychiatr. *88*, 719–726. https://doi.org/10.1016/j.biopsych.2020.03.020.

60. Madden, M.B., Stewart, B.W., White, M.G., Krimmel, S.R., Qadir, H., Barrett, F.S., Seminowicz, D.A., and Mathur, B.N. (2022). A role for the claustrum in cognitive control. Trends Cognit. Sci. *26*, 1133–1152. https://doi.org/10.1016/j.tics.2022.09.006.

61. Krimmel, S.R., White, M.G., Panicker, M.H., Barrett, F.S., Mathur, B.N., and Seminowicz, D.A. (2019). Resting state functional connectivity and cognitive task-related activation of the human claustrum. Neuroimage *196*, 59–67. https://doi.org/10.1016/j.neuroimage.2019.03.075.

62. Ghazisaeidi, S., Muley, M.M., and Salter, M.W. (2023). Neuropathic pain: mechanisms, sex differences, and potential therapies for a global problem. Annu. Rev. Pharmacol. Toxicol. *63*, 565–583. https://doi.org/10.1146/annurev-pharmtox-051421-112259.

63. Bartley, E.J., and Fillingim, R.B. (2013). Sex differences in pain: a brief review of clinical and experimental findings. Br. J. Anaesth. *111*, 52–58. https://doi.org/10.1093/bja/aet127.

64. Mogil, J.S. (2020). Qualitative sex differences in pain processing: emerging evidence of a biased literature. Nat. Rev. Neurosci. *21*, 353–365. https://doi.org/10.1038/s41583-020-0310-6.

65. Aloisi, A.M. (2003). Gonadal hormones and sex differences in pain reactivity. Clin. J. Pain *19*, 168–174.

66. Fodoulian, L., Gschwend, O., Huber, C., Mutel, S., Salazar, R.F., Leone, R., Renfer, J.-R., Ekundayo, K., Rodriguez, I., and Carleton, A. (2020). The Claustrum-Medial Prefrontal Cortex Network Controls Attentional Set-Shifting. https://doi.org/10.1101/2020.10.14.339259.

67. Shiers, S., Pradhan, G., Mwirigi, J., Mejia, G., Ahmad, A., Kroener, S., and Price, T. (2018). Neuropathic pain creates an enduring prefrontal cortex dysfunction corrected by the type II diabetic drug metformin but not by gabapentin. J. Neurosci. *38*, 7337–7350. https://doi.org/10.1523/JNEUROSCI.0713-18.2018.

68. McBride, E.G., Gandhi, S.R., Kuyat, J.R., Ollerenshaw, D.R., Arkhipov, A., Koch, C., and Olsen, S.R. (2023). Influence of claustrum on cortex varies by area, layer, and cell type. Neuron *111*, 275–290.e5. https://doi.org/10.1016/j.neuron.2022.10.026.

69. Pnevmatikakis, E.A., and Giovannucci, A. (2017). NoRMCorre: an online algorithm for piecewise rigid motion correction of calcium imaging data. J. Neurosci. Methods *291*, 83–94. https://doi.org/10.1016/j.jneumeth.2017.07.031.

70. Mayrhofer, J.M., Haiss, F., Haenni, D., Weber, S., Zuend, M., Barrett, M.J.P., Ferrari, K.D., Maechler, P., Saab, A.S., Stobart, J.L., et al. (2015). Design and performance of an ultra-flexible two-photon microscope for in vivo research. Biomed. Opt Express *6*, 4228–4237. https://doi.org/10.1364/BOE.6.004228.

71. Romano, S.A., Pérez-Schuster, V., Jouary, A., Boulanger-Weill, J., Candeo, A., Pietri, T., and Sumbre, G. (2017). An integrated calcium imaging processing toolbox for the analysis of neuronal population dynamics.

PLoS Comput. Biol. *13*, e1005526. https://doi.org/10.1371/journal.pcbi.1005526.

72. Friedrich, J., Zhou, P., and Paninski, L. (2017). Fast online deconvolution of calcium imaging data. PLoS Comput. Biol. *13*, e1005423. https://doi.org/10.1371/journal.pcbi.1005423.

73. Bellone, C., and Nicoll, R.A. (2007). Rapid bidirectional switching of synaptic NMDA receptors. Neuron *55*, 779–785. https://doi.org/10.1016/j.neuron.2007.07.035.

74. Marti Mengual, U., Wybo, W.A.M., Spierenburg, L.J.E., Santello, M., Senn, W., and Nevian, T. (2020). Efficient low-pass dendro-somatic coupling in the apical dendrite of layer 5 pyramidal neurons in the anterior cingulate cortex. J. Neurosci. *40*, 8799–8815. https://doi.org/10.1523/JNEUROSCI.3028-19.2020.

75. Blom, S.M., Pfister, J.P., Santello, M., Senn, W., and Nevian, T. (2014). Nerve injury-induced neuropathic pain causes disinhibition of the anterior cingulate cortex. J. Neurosci. *34*, 5754–5764. https://doi.org/10.1523/JNEUROSCI.3667-13.2014.

STAR★METHODS

KEY RESOURCES TABLE

REAGENT or RESOURCE	SOURCE	IDENTIFIER
Bacterial and virus strains		
AAV-retro-hSyn1-Cre-mCherry	VVF	v147-retro
AAV1-hSyn1-DIO-hM4D-mCitrine	VVF	v93-1
AAV1-hSyn1-DIO-GCaMP6f	VVF	v730-1
AAV1-CaMKIIa-GCaMP6f	VVF	v183-1
AAV2-hEF1α-DIO-ChR2-EYFP	VVF	v214-2
Chemicals, peptides, and recombinant proteins		
Complete Freund's Adjuvant (CFA)	Aviva Systems Biology	Cat#OORA00327
Clozapine-*N*-Oxide (CNO)	Tocris	Cat#6329
Alexa Fluor 405 Streptavidin	Thermo Fisher	Cat#S32351
Alexa Fluor 488 Streptavidin	Thermo Fisher	Cat#S11223
Alexa Fluor 594 Streptavidin	Thermo Fisher	Cat#S11227
Paraformaldehyde (PFA)	Sigma Aldrich	Cat#1004960700
Triton X-100	Sigma Aldrich	Cat#X100-100ML
Mowiol 4-88	Sigma Aldrich	Cat#81381-50G
Experimental models: Organisms/strains		
C57Bl/6J	Janvier Labs	C57Bl/6J
Software and algorithms		
MATLAB	MathWorks	N/A
NoRMCorre	Pnevmatikakis and Giovannucci, 2017[69]	N/A
Igor Pro	WaveMetrics	N/A
Graphpad Prism	Dotmatics	N/A

RESOURCE AVAILABILITY

Lead contact

Further information and requests for resources and reagents should be directed to and will be fulfilled by the lead contact, Thomas Nevian (thomas.nevian@unibe.ch).

Materials availability

This study did not generate new unique reagents.

Data and code availability

- All data reported in this paper will be shared by the lead contact upon request.
- This paper does not report original code.
- Any additional information required to reanalyze the data reported in this paper is available from the lead contact upon request.

EXPERIMENTAL MODEL AND SUBJECT DETAILS

All experiments were carried out in accordance with the guidelines from the veterinary office of the Canton of Bern (Switzerland). Adult (>6 weeks) male C57Bl/6J mice (Janvier Labs), group-housed (unless otherwise specified) with 2–4 littermates under a 12 h light/dark cycle, were used for all experiments. All surgical procedures were performed under isoflurane anesthesia (5% for induction and 2% for maintenance) and constant body temperature monitoring.

METHOD DETAILS

Virus injections

A standard stereotaxic frame (Kopf Instruments) was used to take anteroposterior and mediolateral coordinates (relative to bregma) as well as dorsoventral coordinates (from the pial surface) for intracranial injections. Respectively, these coordinates were (in mm) +1, ±0.35, −1.25 for ACC injections, and +1.1, ±3.1, −2.7 for the claustrum. Virus solutions containing AAV-retro-hSyn1-Cre-mCherry (200 nL), AAV1-hSyn1-DIO-hM4D-mCitrine (100 nL), AAV1-hSyn1-DIO-GCaMP6f (100 nL), AAV1-CaMKIIa-GCaMP6f (200 nL), or AAV2- hEF1α-DIO-ChR2-EYFP (100 nL) were slowly injected through heat-pulled glass pipettes connected to a Picospritzer pressure microinjector (100–200 nL/min, Parker). Viruses were injected unilaterally for electrophysiological and two-photon experiments, or bilaterally for behavioral experiments. After surgery, viral constructs were allowed to express, and mice allowed to recover for at least 3–4 weeks before experimentation. All viruses were purchased from the Viral Vector Facility (VVF) of the University of Zurich.

Pain induction and behavioral testing

Inflammatory pain was induced by injecting 30 μL complete Freund's adjuvant (CFA, Aviva Systems Biology) into the plantar surface of the hind paw contralateral to the hemisphere to be imaged *in vivo* or patched *ex vivo*. To assess the ensuing inflammation-induced mechanical allodynia, mice were individually confined in a plexiglass chamber placed on an elevated grid, where they habituated for 20 min before testing. A von Frey filament was slowly pressed against the plantar surface of either hind paw, and the gram-force needed to elicit a paw withdrawal or flinching was measured with an electronic aesthesiometer (IITC Life Science). For a single session, the mean withdrawal threshold of each paw was averaged from six repeated measurements. For chemogenetic experiments, saline or clozapine-*N*-oxide (CNO, 2 mg/mL) were injected i.p. immediately before habituation. In the repeated von Frey testing from Figure 4, sessions were carried out at least 3 h apart, to maximize intersession CNO clearance. Thermal hyperalgesia was assessed with the hot water test and acetone test. In both assays, mice undergoing inflammatory pain were injected i.p. with 2 mg/mL CNO (or saline) and placed in a transparent plexiglass chamber over a grid floor. After 20 min, 0.1 mL of either 80–85°C water or acetone was applied to the inflamed hindpaw, and the time spent biting, licking, and flinching their paw was recorded and later manually quantified at half speed to measure the coping time within the first minute from paw stimulation. Four hours later, animals were injected with saline (or CNO) and the assay was repeated so that each animal got tested in both conditions. To examine the potential relief from spontaneous CFA-induced inflammatory pain, we performed a conditioned place preference test (CPP)[25] consisting of a pretest, two conditioning sessions, and a test phase. During pretest, mice freely explored a classical CPP apparatus (two 25 cm × 25cm chambers connected by a 10 cm × 7 cm corridor) for 20 min. The chambers were differentiated by visual (striped or dotted walls) and olfactory cues (1% acetic acid or ethanol-based cleanser). After pretest, all mice received an intraplantar CFA injection and returned to their homecages for 24 h. During conditioning, animals received i.p. saline (or CNO) 20 min before being confined in one of the two chambers for an additional 20 min. Four hours later they were given i.p. CNO (or saline) and confined in the other chamber. The least explored chamber during pretest was selected as the CNO-conditioning chamber, whereas the conditioning order was assigned randomly. Four hours after the final conditioning session, animals were allowed free access to the apparatus for 20 min and the normalized difference in time spent in the CNO-paired chamber (T_{CNO}) compared to the saline-paired one (T_{SAL}) was computed as Preference score $= (T_{CNO} - T_{SAL}) / (T_{CNO} + T_{SAL})$. The change in preference score was then calculated by subtracting the score obtained from the pretest to evaluate the emergence of CNO-conditioned place preference (positive values) or avoidance (negative values). All CPP data was recorded and analyzed with Ethovision software (Noldus).

GRIN lens implantation

Long (0.5-mm wide, 6.52-mm long) and short (1-mm wide, 4.38-mm long) gradient-index (GRIN) lenses (Grintech) were respectively employed for the chronic optical access to claustrum and ACC neurons *in vivo*. At the anteroposterior and mediolateral coordinates where the GCaMP6f-encoding virus was injected, a circular craniotomy was performed and the dura mater carefully excised. After cleaning the exposed brain with saline and stopping all bleeding, a gradient-index (GRIN) lens was stereotactically inserted very slowly into the craniotomy (0.2 mm/min) until positioned 200 μm dorsal to the virus injection site. Here, the lens was sealed to the edge of the craniotomy with a self-cure dental adhesive (Super-Bond C), while a short pipette tip segment was cut and laid around the exposed lens and used as an open protective cap. A small screw was then inserted superficially on the parietal bone and, after gently scratching the skull surface for better adhesion, both screw and protective cap were anchored to the scalp with regular cyanoacrylate glue. Finally, the whole implant was secured with a thick layer of Paladur dental cement (Kulzer), covering up to edge of the protective cap. After at least three weeks from surgery, and before the first imaging session, a small, custom-made metal bar to be used for head-fixation under the two-photon microscope was cemented above the implant with Paladur. After mounting the head bars, mice had to be housed individually to minimize the risk of implant removal by cage littermates.

Two-photon microscopy

Calcium imaging data was acquired with a custom-built galvanometric two-photon laser scanning microscope,[70] equipped with a Mai Tai Ti:Sapphire laser (Spectra Physics), a Pockels cell (Conoptics), and a W Plan-Apochromat 20× objective (Zeiss). GRIN lens-implanted animals were lightly anesthetized (0.5%–1% isoflurane) and head-fixed beneath the microscope, where GCaMP6f

was excited at 920 nm and its emitted fluorescence detected by a photomultiplier tube (Hamamatsu). Microscope acquisition and storage was controlled with Scanimage software, and the recorded time series were later analyzed with custom software on MATLAB, Python, and R. In each animal, one or two distinct fields of view, at least 100 μm apart, were imaged at a 3× magnification and recorded at 9.048 frames per second. In the ACC, 40–60 neurons per field of view (FOV) were recorded simultaneously—substantially more than in the claustrum (10–20 neurons) due to its thin structure, incomplete retrograde labeling and conditional GCaMP6f expression. Each FOV went through a 10-min spontaneous activity imaging session followed by three imaging sessions where stimulus-evoked responses were recorded. Stimuli consisted of an electrical foot shock directly applied to the hind paw (FS; 10 mA, 50 ms), an air puff blown 1 cm from the eye (AP; 20 PSI, 500 ms), and burst of white noise through a loudspeaker (WN; 75 dB, 1 s), each being individually administered every 20 s for 10 min. Both FS and AP were delivered contralaterally to the imaged hemisphere (and ipsilaterally to the CFA- or saline-injected hind paw). Time series recorded from each FOV were motion corrected with the NoRMCorre algorithm,[69] and then regions of interest (ROIs) were manually selected over active neuronal somata identified from the time series' cross-correlated projections. To measure relative fluorescence changes ($\Delta F/F_0$), a running-window average of the eighth percentile fluorescence values over an interval 40 times larger than GCaMP6f's decay time constant was used to estimate the baseline fluorescence F_0[71]. Calcium transients were detected with a continuous wavelet transform-guided event-detection algorithm, and the underlying spike trains were inferred using the OASIS toolbox in MATLAB.[72] A logistic regression classifier was used to identify stimulus-responsive neurons. In each trial (30 for each stimulus), the inferred spikes were binned and compared to a bootstrapped distribution in order to evaluate significant neuronal activations, and to determine peak activity latencies and response durations. Stimulus responsiveness was then determined based on the area under the precision-recall curve given by the classifier. Calcium responses were quantified as the area under the curve (AUC) of the $\Delta F/F_0$ traces within 5 s from stimulus onset, or during the whole 10 min of recording for spontaneous activity sessions. To compare changes from pre-stimulus baseline activity across neurons and conditions, $\Delta F/F_0$ signals were Z score normalized in activity heatmaps and example traces. When recording claustrum neurons across multiple days, the same FOVs were imaged to follow the dynamic changes in stimulus-selectivity within each animal. For chemogenetic experiments, basal spontaneous and stimulus-evoked sessions were acquired before an i.p. injection of 2 mg/kg CNO or saline. Fifteen minutes later, all sessions were acquired a second time to examine the average neuronal activity change for each neuron with the formula $activity\ change = 100 * (AUC_{post} - AUC_{pre})/AUC_{pre}$, where AUC_{pre} and AUC_{post} represent the calcium activity during baseline and post-injection recording sessions, respectively.

Electrophysiology

Coronal brain sections (300 μm) were cut on a vibratome in an ice-cold slicing solution containing, in mM: 65 NaCl, 2.5 KCl, 25 $NaHCO_3$, 1.25 NaH_2PO_4, 7 $MgCl_2$, 0.5 $CaCl_2$, 25 glucose, and 105 sucrose. ACC and claustrum-containing slices (1.1–0.2 mm anterior to bregma) were transferred to a recovery chamber filled with 30°C warm artificial cerebrospinal fluid (aCSF) containing, in mM: 125 NaCl, 2.5 KCl, 25 $NaHCO_3$, 1.25 NaH_2PO_4, 1 $MgCl_2$, 2 $CaCl_2$, and 25 glucose. After a 20-min incubation at 30°C, slices were allowed to reach room temperature and recover for at least 30 min before being transferred to the recording chamber, superfused with 30°C aCSF at a [2 mL/min] flow. All solutions used were constantly bubbled with a gas mixture of 95% O_2 and 5% CO_2. Whole-cell patch clamp recordings were performed using heat-pulled borosilicate glass pipettes with a tip resistance of 4–7 MΩ. For current clamp experiments, the internal solution contained, in mM: 130 K-gluconate, 5 KCl, 10 Na-phosphocreatine, 4 Mg-ATP, 0.3 Na-GTP, and 10 HEPES. Voltage clamp experiments were performed with an internal solution containing, in mM: 125 gluconic acid, 130 CsOH, 5 CsCl, 10 Na-phosphocreatine, 4, Mg-ATP, 0.3 Na-GTP, 10 HEPES, 0.1 spermine, and 5 QX-314. All internal solutions also contained 2 mg/mL biocytin for post hoc neuronal reconstruction. Neurons were visualized through an IR CCD camera mounted on a Leica DM LFSA microscope equipped with LEDs for fluorophore excitation, optical ChR2 stimulation, and infrared sample illumination (Thorlabs). Currents were filtered at 5 kHz and amplified, then digitized at 10 kHz and stored on a computer. Custom-made Igor Pro procedures (WaveMetrics) were used for all data acquisition and analysis. For the *ex vivo* validation of chemogenetic experiments, 10 μM CNO was added to the aCSF. To confirm the monosynaptic nature of claustrum-ACC connections, action potential-dependent transmission was abolished with 1μM TTX, and ChR2-induced depolarization broadened with 0.5 mM 4-AP.[26] $GABA_A$-mediated transmission was blocked with 10 μM gabazine, whereas AMPA and NMDA receptors were blocked with 10 μM CNQX and 50 μM AP5, respectively. All compounds were bath-applied for at least 10 min before assessing drug effects. During current clamp experiments, series of increasing (0–1 nA), 500-ms long current steps were delivered to determine the neuronal input-output function as a measure of intrinsic excitability. In voltage clamp experiments, ChR2 was stimulated with 5-ms blue light pulses delivered through the microscope objective by a 470 nm LED. All currents were analyzed from the average of at least 20 consecutive traces, each being recorded every 10 s. To record $GABA_A$-mediated currents, neurons were recorded at 0 mV and IPSCs were obtained from digital subtraction of the gabazine-resistant traces. Similarly, NMDA traces were obtained by subtracting the AP5-resistant traces from the currents recorded at +40 mV. A threshold of four standard deviations from baseline noise was used to determine the postsynaptic current onset (relative to optical stimulation). To assess changes in short term plasticity, paired pulses were delivered at 20 Hz, and the peak of the second current divided by the first to obtain the paired-pulse ratio. To evaluate the degree AMPA receptor rectification, EPSCs were recorded in 10 μM gabazine and 50 μM AP5 at +40, 0, and −70 mV, and their rectification index was calculated as the ratio of the chord conductances measured at negative and positive potentials. To gauge NMDA subunit changes, weighted decay time constants of isolated NMDA-mediated currents were calculated from their peak-normalized area under the curve, from peak to 90% current decay.[73] Average numbers and conductances of open synaptic AMPA channels were

estimated with a nonstationary fluctuation analysis,[27] whereby individual EPSC traces were peak scaled to their mean current, and their variance around the mean during the decay phase was binned and plotted against the mean current amplitude. The resulting parabolic relationship was fitted by the equation: $\sigma^2 = iI - I^2/N + b$, where σ^2 is the variance around the mean current, b is the background variance, I is the mean current, N is the estimated number of open channels at peak current, and i is the estimated unitary channel current. The corresponding unitary channel conductance (γ) was then retrieved from the relationship $\gamma = i/\Delta V$, where $\Delta V = holding\ potential - reversal\ potential$.

Histology

Mice used for *in vivo* imaging and behavioral experiments were terminally anesthetized with a saline mixture of 200 mg/kg ketamine and 20 mg/kg xylazine before being transcardially perfused with 0.1 M PBS followed by 4% paraformaldehyde (PFA). Brains were removed, postfixed in 4% PFA and then cut in 100 μm-thick sections on a vibratome. Slices were then mounted on glass slides with an antifading mounting medium (Enzo) and injection sites, viral expression, and implant locations were examined on a Leica M205 FCA stereomicroscope. At the end of *ex vivo* patch clamp experiments, the recording pipette was slowly retracted, and the brain slice was fixed in 4% PFA at 4°C overnight for reconstruction. After washing the slices with PBS (3× for 10 min), they were permeabilized in PBS containing 2% Triton X-100 for 1 h. Then slices were incubated with streptavidin-conjugated Alexa 488/Alexa 594/Alexa 405 (1:200; Thermo Fisher) in PBS containing 1% Triton X-100 depending on the fluorescence tag. After washing with PBS (3× for 10 min), the processed slices were embedded in custom-made antifade based on Mowiol (Sigma Aldrich) on microscopy slides. For morphological reconstruction, fluorescently labeled cells were imaged using a confocal microscope (Leica Microsystems, SP8) equipped with a white-light laser and two GaAsP-detectors (HyD). Imaging was performed with a 20× objective (Leica Microsystems, HC PL APO, 20×, NA 0.75 IMM CORR CS2).[74,75]

QUANTIFICATION AND STATISTICAL ANALYSIS

All data was presented as mean ± s.e.m. or as boxplots representing the median, interquartile range, and whiskers delimiting the 10th and 90th percentiles. Differences between groups were evaluated as reported in the figure legends using GraphPad Prism software and were considered statistically significant for $p < 0.05$.